Archaeological and Anthropological Sciences (2019) 11:1927–1938
https://doi.org/10.1007/s12520-018-0648-0

ORIGINAL PAPER

An assessment of microCT technology for the investigation of charred archaeological parenchyma from house sites at Kuk Swamp, Papua New Guinea

Jenifer Pritchard[1] · Tara Lewis[2] · Levi Beeching[3] · Tim Denham[1]

Received: 20 October 2017 / Accepted: 23 April 2018 / Published online: 4 May 2018

Abstract

Archaeological parenchyma is analysed using microCT to enable virtual histological examination and taxonomic identification to species level. MicroCT images are compared with reflected light microscopy (RLM) and scanning electron microscopy (SEM) images of fresh, desiccated and charred reference specimens. These results reveal differences in cell dimensions depending upon sample preparation and highlight the importance of using appropriately prepared reference material. A reference library is provided as supplemental material to address a lack of available imagery of reference specimens. MicroCT analysis confirms previous, more tentative, identifications of fragments of archaeological parenchyma from relatively recent archaeological contexts at Kuk Swamp, highlands of Papua New Guinea. Five archaeobotanical fragments are described in detail and with varying levels of confidence to sugarcane (*Saccharum officinarum*) and sweet potato (*Ipomoea batatas*). The study demonstrates the potential of non-destructive microCT for the identification of archaeological parenchyma.

Keywords Archaeological parenchyma · MicroCT · Virtual histology · Sugarcane (*Saccharum officinarum*) · Sweet potato (*Ipomoea batatas*) · Archaeobotany

Introduction

The taxonomic identification of macrobotanical specimens is an integral part of archaeological research. Archaeological parenchyma is often an under-reported and under-identified component of archaeobotanical assemblages due to difficulties of taxonomic identification and access to suitable reference collections. A combination of reflected light microscopy (RLM), transmitted light microscopy and scanning electron microscopy (SEM) is typically used to describe and identify archaeological parenchyma (Rosendahl and Yen 1971; Ugent et al. 1981; Ugent and Peterson 1988; Hather 1991, 2000; Ladefoged et al. 2005).

In this study, the value of microCT to archaeobotanical investigation is evaluated for five charred archaeological parenchyma samples, comprising macrobotanical culm and tuber remnants previously described using RLM by Lewis et al. (2016). The charred fragments of archaeological parenchyma were obtained during excavations of house sites and associated contexts at Kuk Swamp, Papua New Guinea in 1972 and 1973. Two of these were previously identified with different levels of confidence: one fragment (20.2) was identified to *Saccharum officinarum* L.; another (fragment 61.9) was identified as probable *Ipomoea batatas* (L.) Lam.; while taxonomic determinations were not possible for the other three fragments. Here, virtual histological transects show the internal cellular structures of these archaeobotanical samples and enable more secure taxonomic determinations.

Archaeological parenchyma

Archaeological parenchyma is a general term that refers to the soft parenchymatous tissue of plants preserved at

Electronic supplementary material The online version of this article (https://doi.org/10.1007/s12520-018-0648-0) contains supplementary material, which is available to authorized users.

✉ Tim Denham
Tim.Denham@anu.edu.au

[1] College of Arts and Social Science, Australian National University, Canberra, Australia

[2] School of Life and Environmental Sciences, Deakin University, Geelong, Australia

[3] Department of Applied Mathematics, Australian National University, Canberra, Australia

archaeological sites, usually in charred or desiccated form (Hather 1988, 2000). The analysis and identification of archaeological parenchyma is a technique which has not been widely adopted in archaeobotany, although studies have occurred in the Americas, Europe and the Indo-Pacific region (for example, Ugent et al. 1981; Ugent and Peterson 1988; Hather 1994a; Hather and Kirch 1991; Paz 2001; Oliveira 2008). For the wet tropics, the analysis of archaeological parenchyma was originally considered a technique to identify forms of cultivation based on the vegetative propagation of crops (Hather 1992, 1994b, 1996).

Many staples under vegetative forms of cultivation in the Indo-Pacific region do not yield hard woody tissues, nut shells or seeds that ordinarily preserve well in archaeological contexts. Most root crops—such as yams (*Dioscorea* spp.), taro (*Colocasia esculenta*), sweet potato (*Ipomoea batatas*) and manioc (*Manihot esculenta*), as well as vegetative crops such as bananas (*Musa* spp.), sugarcane (*Saccharum officinarum*) and other plants—are usually harvested prior to flowering or seed-set. Consequently, the interpretation of past cultivation of these crops has been based on starch grain and phytolith analysis (Denham et al. 2003), as well as to a limited extent upon archaeological parenchyma (Lewis et al. 2016).

In the Indo-Pacific region, the analysis of archaeological parenchyma is currently an under-utilised archaeobotanical method for the investigation of cultivation and domestication in the past (Denham et al. 2009). Here, the application of microCT to the investigation of archaeological parenchyma is evaluated through the analysis of samples from relatively recent domestic contexts in highland Papua New Guinea. The utility of the technique for anatomical description and taxonomic identification is assessed, and its value for the future establishment of online, virtual reference collections is considered.

Methods

Archaeobotanical fragments

Fragments of archaeological parenchyma were recovered during the excavation of domestic and associated contexts dating to the last few hundred years on the wetland margin at Kuk Swamp in the highlands of Papua New Guinea (Lewis et al. 2016; Golson et al. 2017). The five fragments reported here comprise two fragments (Fr.20.2 and Fr.20.6) from a field ditch (feature 27) pre-dating house construction; two fragments (Fr.14.1 and Fr.61.9) from a shallow ditch (recorded as features 30 and 32) dug to enhance drainage around a house (house Q); and one fragment (fragment16.3) from a fireplace in a slightly later house (house B) (Table 1, with descriptive detail of fragments in Online Resource Table 1 and Online Resource Figs. 1, 2 and 3). All features post-date AD 1640.

A major disadvantage of standard histological examination (undertaken here for modern reference specimens) is the necessary partial or complete destruction of archaeobotanical fragments during sample preparation, whether cutting and slide mounting for histological analysis or the creation of clean and smooth fracture planes for SEM analysis (Hather 2000: 75–77). Sample preparation eliminates the possibility of re-examination following methodological refinements or the development of new technologies and theories. Here, imaging by X-ray micro computed tomography with micron-scale, and potentially sub-micron, resolution (microCT; Varslot et al. 2011) permits non-destructive digital analysis of surface and internal features within fragments of archaeological parenchyma. Furthermore, microCT enables the 3D visualisation and virtual histological analysis of entire samples, whereas traditional methods of investigation enable effective 2D visualisation and analysis (even though SEM provides greater depth of field than standard optical techniques). Recent applications of microCT analysis to archaeological and palaeoecological samples include bone (Booth et al. 2016), portable art in bone and antler (Bello et al. 2013), wood anatomy (Haneca et al. 2012; Whitau et al. 2016), dendrochronology (Stelzner and Million 2015), sediments (Edwards et al. 2017) and rice (*Oryza sativa*) inclusions in pottery (Barron et al. 2017).

Modern reference specimens

The list of species and specimens analysed here are given in Online Resource Table 2. Samples of dried reference culm node and internode of selected cane grasses and a tuber of *Dioscorea nummularia* Lam. (as a representative yam) were obtained from the Australian National Herbarium. In addition, fresh tubers of sweet potato (*Ipomoea batatas*) and dried culm sections of sugarcane mulch (*Saccharum officinarum*) were obtained commercially.

Macrobotanical materials preserved in the archaeological record through desiccation or charring may be altered and distorted in morphological and histological dimensions. Talbot and White (2013) report that the usual methods of preparation of plant material for microscopy with chemical fixation and critical point drying (CPD) can reduce cellular dimensions up to 30%. These factors necessitate comparative analyses of reference plant tissues prepared and imaged under different conditions to approximate past conditions of archaeobotanical preservation.

Reference specimens of *Saccharum officinarum* L., *Bambusa solomonensis* Holttum and *Bambusa vulgaris* Schrad. ex J.C. Wendl. (accession numbers CANB 683035, CANB 149008 and CANB 321827 respectively) were embedded in epoxy resin and cut with a rotating diamond saw to expose transverse and longitudinal stem sections. These

Table 1 Provenance and radiocarbon dating information for archaeobotanical remains. Calibrations were undertaken using the IntCal13 calibration curve (Reimer et al. 2013) in Calib v.7.1 (Stuiver et al. 2005). Wk-31780, Wk-34108 and Wk-34109 previously reported in Lewis et al. (2016). ANU-16906 and ANU-16907 are archaeobotanical fragments 20.5 and 20.6, respectively. Antiquity of feature 27 field ditch is more recent than reported in Lewis et al. (2016), most likely corresponding to late Kuk phase 5 or early Kuk phase 6, not to Kuk phase 4

Lab code	House site	Bag	Feature	Material	Radiocarbon age (BP)	Calibrated radiocarbon date (cal BP) (95.4%—two sigma)	
ANU-16906	Pre-house antiquity	20	F27, field ditch	Charred unidentified cane grass fragment	225 ± 23	0–11 150–186 271–307	0.079 0.426 0.496
ANU-16907	Pre-house antiquity	20	F27, field ditch	Charred sugarcane fragment (*Saccharum officinarum*)	219 ± 23	0–12 148–187 206–211 269–305	0.102 0.460 0.010 0.428
Wk-31780	House B	16	F38, fireplace in house B	Charred tuber fragment (*Ipomoea batatas*)	151 ± 25	0–37 66–118 125–127 130–154 167–231 244–283	0.186 0.164 0.004 0.111 0.364 0.171
Wk-34108	House Q	14	F30, house Q ditch	Charred tuber fragment (*Ipomoea batatas*)	134 ± 25	9–42 59–151 173–274	0.159 0.436 0.405
Wk-34109	House Q	61	F32, house Q ditch	Charred tuber fragment (*Ipomoea batatas*)	157 ± 26	0–36 68–118 131–155 166–231 244–284	0.189 0.127 0.112 0.398 0.173

surfaces were initially smoothed with wet/dry silicon carbide emery paper in series of 400, 800 and 1200 grit. This was followed by polishing with a Struers Labodoser: first, 8 min on a 6-μm grinding disc lubricated with Kemet 6 μm diamond suspension and paste; then, 8 min on a 3-μm DAC grinding disc lubricated with Kemet 3 μm (WM) diamond suspension and paste; and, 2 min on a 1-μm DUR grinding disc lubricated with Kemet 1 μm (WM) diamond suspension and paste. Specimens were imaged under reflected light microscopy then coated with carbon and imaged by SEM.

Specimens that were too small to prepare by the above method were rehydrated and softened in a 1:1 solution of glycerol: ethanol for 48 h. Transverse sections of node and internode were surfaced using a Leica SM2010R sliding microtome. Specimens were dehydrated in ethanol series increasing by 10% steps for 24 h at each concentration to reach 100% ethanol. This was followed with critical point drying and imaging uncoated by RLM and SEM.

Additional reference specimens were charred in a muffle furnace. Specimens were wrapped in foil, placed into a cold muffle furnace set at 300 °C. The set temperature was reached in approximately 30 min. Specimens were kept at this temperature for 2 h. The furnace was turned off and allowed to cool overnight before specimens were removed and surfaces prepared for imaging by sliding microtome.

Image analysis of modern reference specimens and archaeobotanical fragments

A Leica M80 stereo microscope fitted with IC80 camera or a Leica MZ FLIII stereo microscope fitted with an AxioCam HR3 camera and AxioVision imaging software were used for RLM. A Zeiss EVO 15 scanning electron microscope at 10 to 20 kV accelerating voltage was used for SEM imagery.

The archaeobotanical fragments were scanned whole at the 'National Laboratory for X-ray Micro Computed Tomography (CTLab)' based at the Australian National University (ANU) using a HeliScan MicroCT system to yield images at a resolution of c. 2 μm. The results of the microCT scans were analysed with Drishti (v2.6.3) volume rendering software (Limaye 2012). Each microCT scan was subsampled using the Drishti software to simulate 2D RLM images. Virtual internal transverse and longitudinal sections were created using the Drishti software to simulate SEM images. Analyses of the diagnostic features are given in Online Resource Tables 3, 4, 6 and 10. All cell dimensions were measured using AxioVision LE 4.8.2 SP3 Release 08-2013 imaging software. Cell dimensions are given in microns and are tabulated in Online Resource Tables 5, 7, 8 and 9. Cell walls were measured between adjacent cells and divided in half to determine single cell wall thickness. Statistical analyses

of cell dimensions were carried out using standard single-factor ANOVA tests in Microsoft Excel.

Results

Desiccated and charred reference specimens

RLM and SEM images of sugarcane reference specimens (Online Resource Fig. 4) show the variation that can occur between samples. The desiccated sugarcane mulch has essentially retained its histological detail after charring. The internode pith parenchyma cell wall thickness was 9.5 ± 2.3 μm in the dried herbarium sample, 10.8 ± 2.1 μm in the dried sugarcane mulch and 7.4 ± 1.4 μm in the charred mulch (Online Resource Table 7). A single-factor ANOVA found no significant differences between the internode pith parenchyma cell wall thickness or the internode parenchyma cell length of the desiccated herbarium sample and the dry sugarcane mulch. This result would suggest that these parameters do not vary significantly within a range of culm diameters from 9 mm to 3 cm. However, a significant difference was found between the dry and the charred sugarcane mulch for both parameters where the dimensions from the charred sample were smaller. This finding reinforces the need to use appropriately treated reference material for comparison with archaeological samples.

The reference *Dioscorea nummularia* CANB 170079-170080 tuber (Online Resource Fig. 5) has retained its histological integrity after charring. This may be due in part to the fact that the sugarcane and *Dioscorea* samples were already desiccated and are very fibrous in nature. These factors may fix the cell structure and partially protect against charring. The charred reference *D. nummularia* parenchyma average cell wall thickness is 1.5 ± 0.37 μm (Online Resource Table 9). The cell wall thickness of the parenchymatous tissue of *Dioscorea esculenta* (Lour.) Burkill is less than 0.5 μm thick under light microscopy (Horrocks et al. 2008). More measurements are required from other *Dioscorea* species tubers to determine the full range of variation for parenchyma cell wall thickness.

In contrast, under identical conditions, the charred fresh sweet potato is dramatically altered and resembles descriptions by Ladefoged et al. (2005: 367) "with only limited visibility of individual cell outlines". This contrasts with reports by Ussher (2015) who finds much of the tissue anatomy unchanged when fresh and dried samples were charred. Slightly more damage to the charred fresh samples was observed with some compression in the cortex and separation of the boundary from the conjunctive tissues. The severity of the charring process affects the degree of tissue alteration (Hather 1991; Hather and Kirch 1991).

Online Resource (Fig. 6) demonstrates the alteration of sweet potato as a result of charring. The periderm and cortex has fused, bulged and lifted away from the surface of the sweet potato creating tangentially oriented cavities (Online Resource Figs. 6.4 and 6.5). The cut surface fused and bulged away from the cortex and pith parenchyma (Online Resource Figures 6.6a and S6.7a). Large radially oriented cavities formed within the parenchymatous tissue leave very few of the parenchyma cells intact (Online Resource Figures 6. 7b, 6.5b and 6.5c). Similar cavities formed around vascular strands which have remained (Online Resource Figures 6.7c, 6.7d, 6.8a and 6.8b). All of these distortions are considered typical of charred sweet potato (Hather and Kirch 1991). Hather and Kirch (1991) report that the xylem survives charring while the phloem does not. It may be concluded, therefore, that the vascular strand remaining in the charred reference specimen is xylem.

In fresh sweet potato, the periderm cell wall thickness was estimated to be between 7 and 15 μm determined from a published image by Philpott et al. (2009) and the parenchyma cell wall is approximately 10 μm thick (Antonio et al. 2011). The average periderm cell wall thicknesses obtained from the reference specimens were 8.8 ± 1.9 μm in the fresh tissue, 4 ± 0.7 μm in the ethanol fixed/critical point dried sample and 4 ± 0.7 μm in the charred samples. There were very few discernible periderm cells in the charred tissue and only six measurements were made, while the other averages were derived from 20 measurements. The average parenchyma cell wall thickness in the fresh reference sample was 11.6 ± 2.0 μm, 1.5 ± 0.5 μm in the ethanol-fixed/critical point dried sample and 10.7 ± 2.0 μm in the charred sample (Online Resource Table 9). A single-factor ANOVA test found significant differences between fresh and charred periderm cell wall thicknesses but not between fresh and charred parenchyma cell wall thicknesses. However, there was a significant difference with the ethanol-fixed/critical point dried parenchyma cell wall thickness from fresh and charred. A significant difference was found between charred parenchyma cell walls of the sweet potato and *Dioscorea nummularia* samples. This result would suggest that parenchyma cell wall thickness could be a key diagnostic feature for differentiating charred sweet potato from *Dioscorea* tubers in the archaeological record provided the degree of charring is not so severe as to distort the cells to the point of preventing accurate measurements.

Archaeobotanical fragment analysis

MicroCT images of fragment 20.2 from feature 27 demonstrate the superiority of this technique in showing histological detail on all parts of the undulating surface of the fragment (compare Fig. 1 to RLM images in Online Resouce Fig. 7). The analysis of images of virtual transverse and longitudinal sections confirms previously described features and dimensions (Lewis et al. 2016). See

Online Resource Tables 3 and 5 for details of diagnostic features and dimensions measured.

The vascular bundle and bundle sheath shape and orientation within the parenchymatous ground tissue are observable with sufficient resolution to rule out the bamboos examined in the reference samples, as well as bamboo in general (Online Resource Fig. 8 and Table 11 for diagnostic information of the bamboos). A single factor ANOVA finds no significant difference in the internode pith parenchyma cell wall thickness between fragment 20.2 and the charred sugarcane mulch. The results of these analyses are consistent with reference specimens and published descriptions of *Saccharum officinarum* and provide the basis for the highest level of confidence in identification without prefix according to criteria set out by Barton and Paz (2007).

Fragment 20.6 from feature 27 has been subject to RLM and microCT analysis (Fig. 2). The surface layer of the

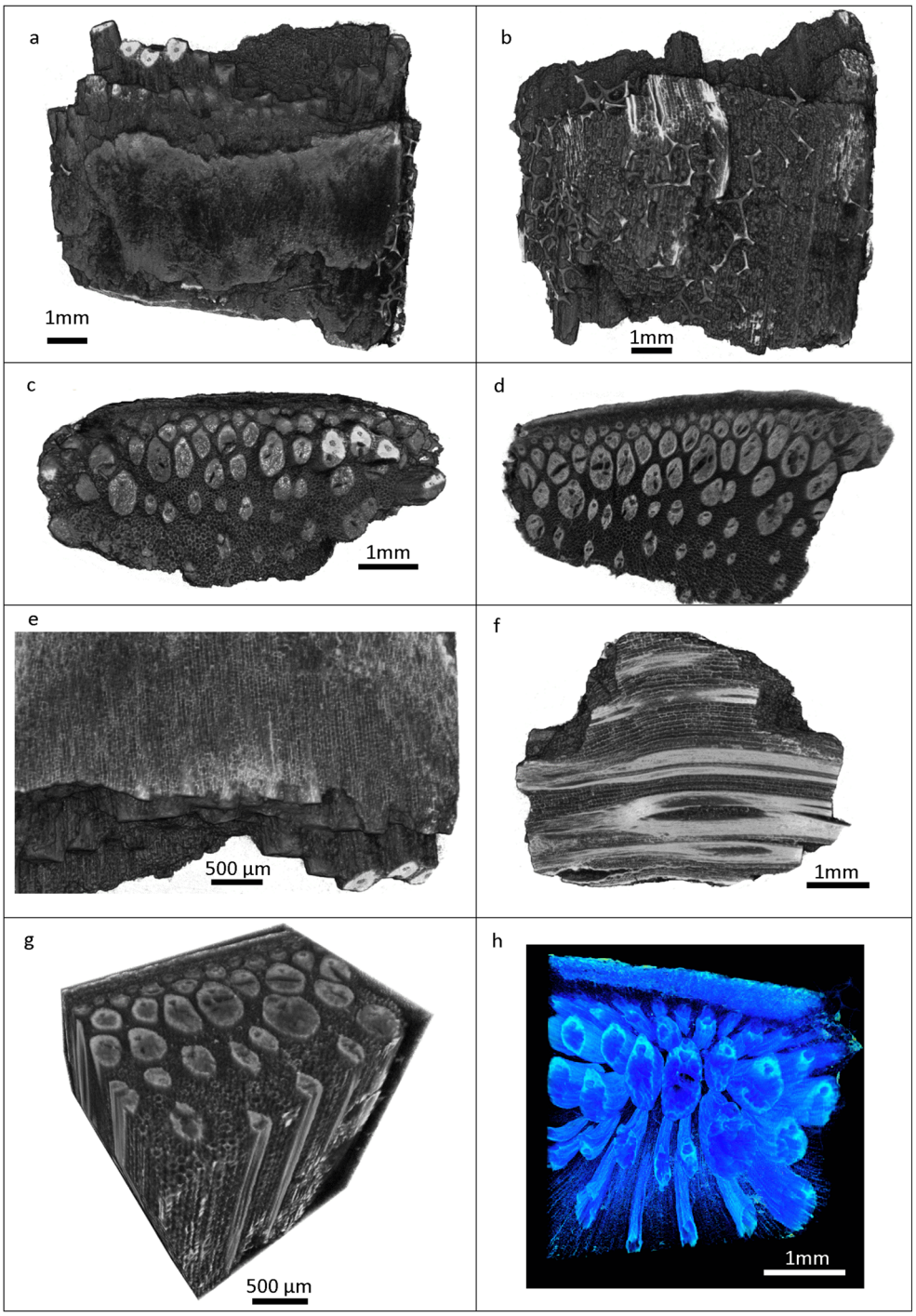

Fig. 1 MicroCT images of Fr20.2, F27. **a** Whole fragment—longitudinal view of outer culm surface showing remnant of rind. **b** Longitudinal view of opposite pith surface. **c** Transverse view of outer surface showing vascular bundle (VB) in cortex near rind. **d** Internal plane—virtual transverse view (TS) showing VB and sclerenchyma (Sc), bundle sheath (BS) ovate throughout culm (ovals less elongated in pith). **e** Cellular detail of cortex below smooth surface of rind remnant in longitudinal view. **f** Internal plane—virtual radial longitudinal section showing layers of sclerenchyma (Sc), parenchyma (Pa) and vascular bundles (VB). **g** Internal structure—virtual 3D transverse longitudinal section. **h** Demonstrating microCT capability to isolate different components within a specimen here components of the bundle sheath and cortex is highlighted

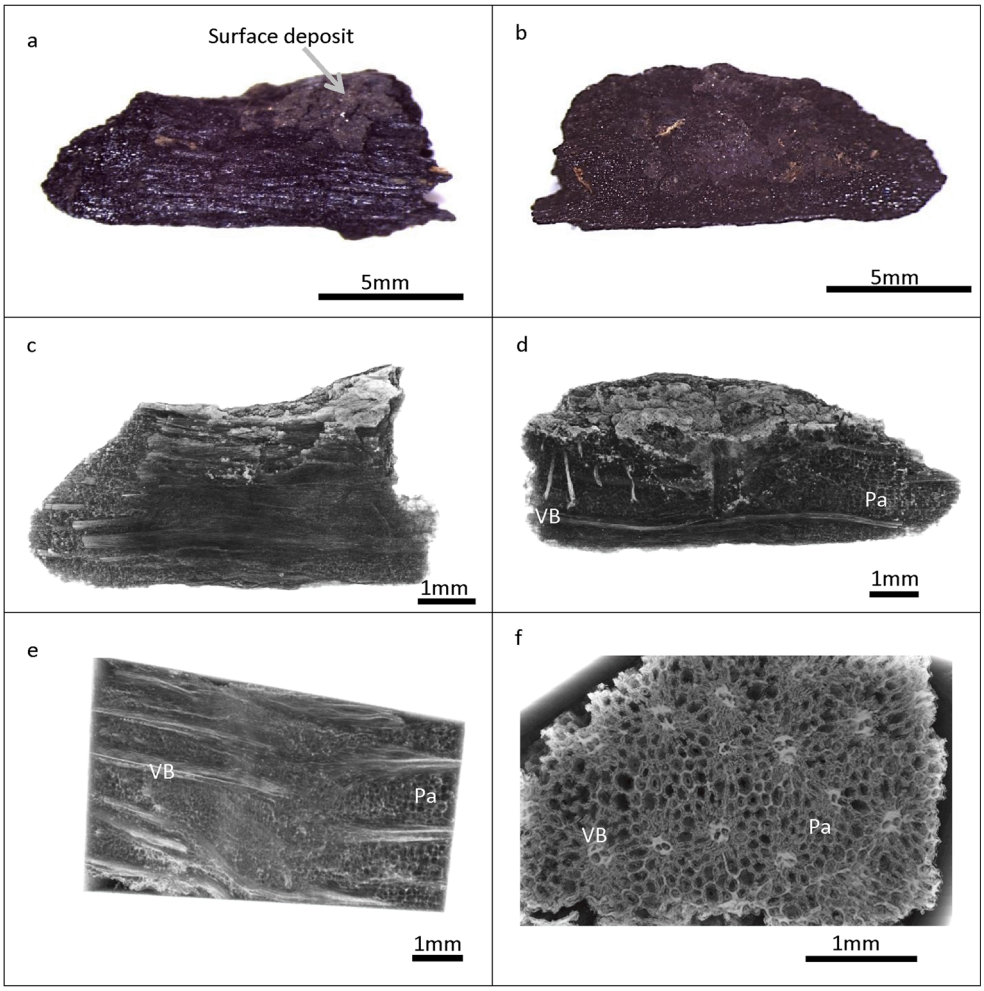

Fig. 2 Images of Fr20.6, F27. RLM photomicrographs of **a**, **b** longitudinal view of whole fragment viewed from different aspects. MicroCT virtual sections of broken fragment: **c** longitudinal view, **d** internal surface—virtual LS showing Pa and VB (note transverse and longitudinal orientations of VB typical of node region), **e** internal surface—deeper into the fragment—showing Pa and VB in different orientations, and **f** virtual transverse section showing shape and orientation of VB in pith Pa and the absence of rind at the margins

fragment is without cellular detail in the microCT images. There may be a deposit of some kind, or possible fusion of the outer layers by charring. However, the consistent uniform configuration of the vascular bundles, bundle sheaths and their spatial arrangement within the ground parenchyma tissue in virtual transverse view (Fig. 2f) would indicate that this is probably a fragment of sugarcane pith without the culm periphery. In addition, the virtual longitudinal views in Fig. 2d, e show the vascular tissue is oriented in different planes throughout the culm which suggest this fragment is most likely from the node region of the culm. See Online Resource Tables 7 and 8 for details of observations and measurements made. In this case, a single-factor ANOVA found no significant difference between the pith parenchyma cell wall thickness of fragment 20.6 and the desiccated reference *S. officinarum* herbarium sample or the desiccated sugarcane mulch, but did find a significant difference with the charred sugarcane mulch. Given that the histological configuration resembles *S. officinarum* so closely, this result suggests that fragment 20.6 is not as severely charred as fragment 20.2.

Fragment 61.9 from feature 32 shows features that are consistent with the characteristics of charred sweet potato (Fig. 3). Multiple radially oriented charred cavities sit within radially oriented fused parenchymatous cells below a band of fused tangentially oriented cells at the surface (Fig. 3a–c, with Fig. 3d–f showing microCT analysis) which is typical of charred sweet potato. Fragment 61.9 is also of sufficient dimensions to contain vascular tissue. There is evidence of a ring of vascular tissue bordering the parenchymatous region within the tangentially oriented cells that run longitudinally parallel to the outer margin (Fig. 3e), which resembles the ordered vascular arrangement of sweet potato. The proximity of this vascular ring to the outer margin of the fragment would suggest that the periderm and much of the cortex has been fused or removed as a result of charring. While examination of the entire fragment in virtual transverse sections does not reveal signs of the characteristic circular cell pattern of secondary growth noted in sweet potato, there is no evidence of randomly distributed vascular bundles in the parenchymatous region that would be expected in *Dioscorea*.

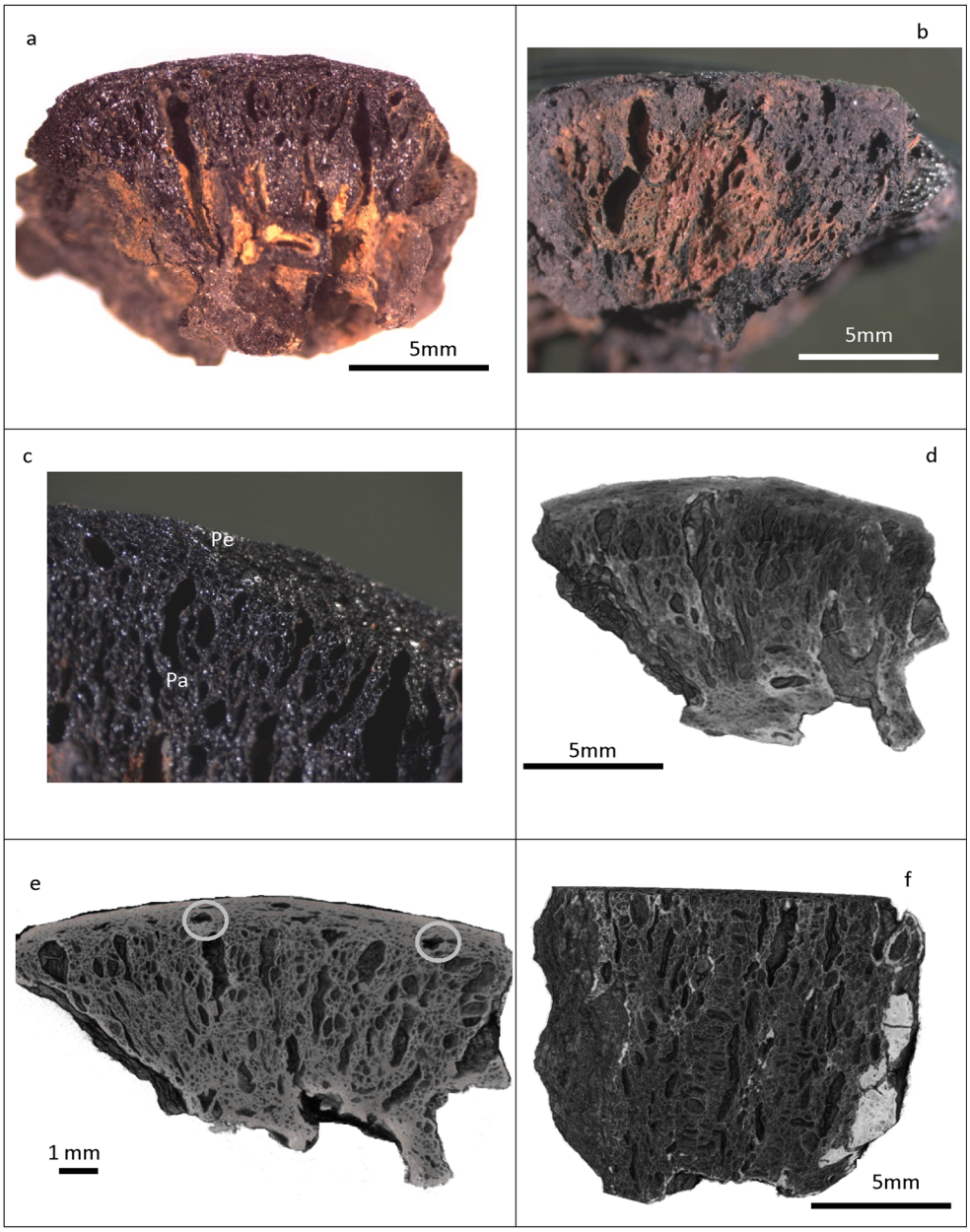

Fig. 3 Images of Fr61.9, F32. RLM photomicrographs of **a** transverse view of entire fragment outer surface from one orientation, **b** view of opposite parallel face, **c** transverse view of fused and distorted cells in charred periderm bordering radially oriented cavities in inner parenchyma at higher magnification. MicroCT virtual images of **d** transverse view of whole fragment outer surface showing radially oriented cavities created by charring, **e** internal plane—virtual TS showing remnants of xylem in tangentially oriented cambium layer (circled), and **f** internal plane—virtual LS showing longitudinally oriented cavities created by charring

A single factor ANOVA test found a significant difference with the charred reference material in periderm/cortex and parenchyma cell wall thicknesses. The degree of cell fusion created by charring leaves very few intact cells that can be measured to accurately determine histological metrics on this fragment (Fig. 3c, e), which makes accord with reference specimen measurements difficult using metric analysis. Even so, the morphological features would rule out species of *Dioscorea* and suggest a dicotyledonous underground storage organ (USO) such as sweet potato.

The overall anatomy of fragment 14.1 from feature 30 is consistent with that of charred sweet potato (Fig. 4). A single factor ANOVA test found a significant difference in parenchyma cell wall thicknesses between the archaeobotanical sample and charred reference material. However, microCT images (Fig. 4c–d) show a multilayered cortex bordered by a vascular strand running parallel to the surface which separates the cortex and parenchymatous tissue. A section of the outer cell layers is bulging and peeling away at the surface (Fig. 4d). The charring pattern of radially oriented cavities (Fig. 4e) resembles that described for sweet potato. In addition, examination throughout the entire fragment in transverse view revealed two regions of circular cellular arrangements with "parallel elongated vesicles suggesting a radial orientation in underlying cell structure", (Fig. 4f; Ladefoged et al. 2005:368) typical of sweet potato.

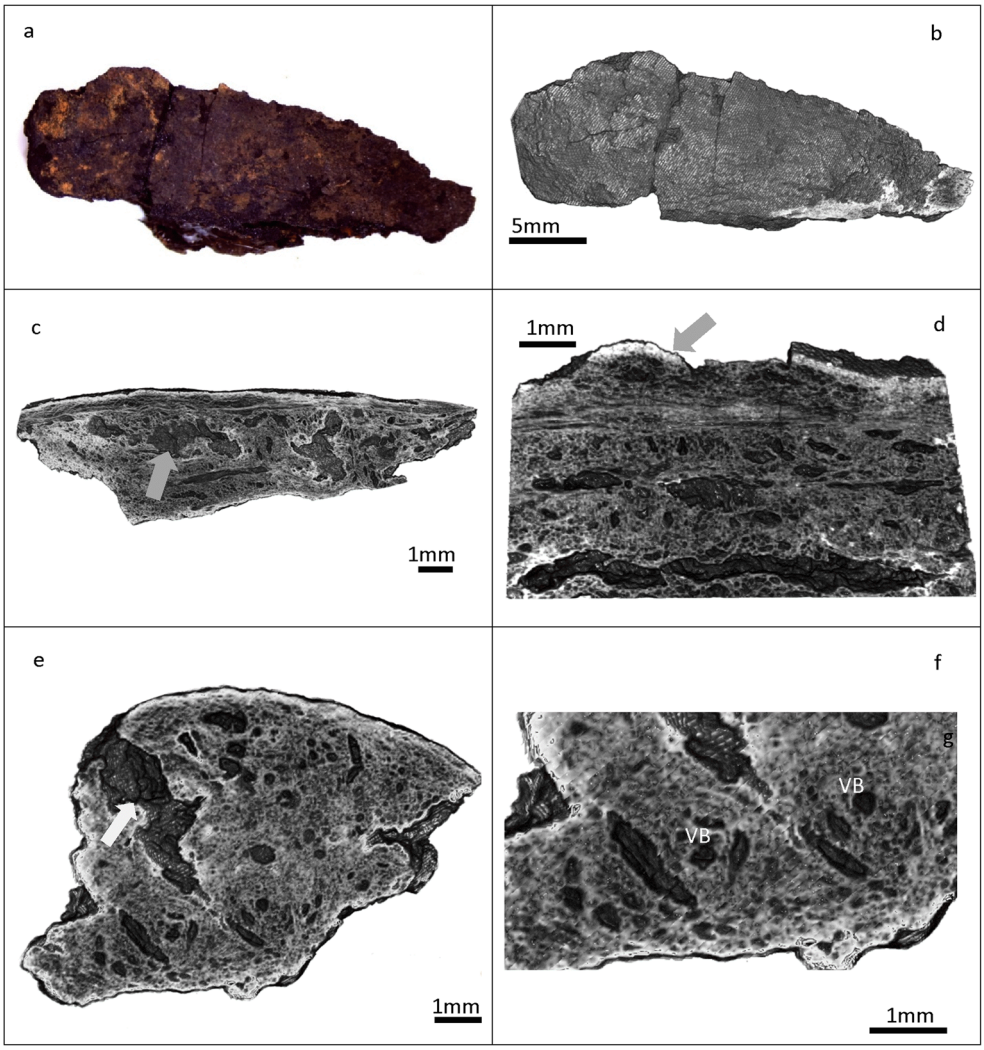

Fig. 4 Images of Fr14.1, F30. RLM photomicrograph of **a** longitudinal view of whole fragment showing external periderm. MicroCT images of **b** same longitudinal view of whole fragment exterior, **c** internal surface full length—virtual LS showing cavities created by charring (arrow), **d** internal surface—virtual LS and periderm/cortex lifting away from surface (arrow), **e** internal surface—virtual TS showing cavities created by charring, and **f** internal surface—virtual TS showing circular cellular arrangement suggestive of secondary cambial growth around VB

The entire length of fragment 16.3 from feature 38 exhibits two recognisable xylem strands within the pith parenchymatous tissue. A characteristic charring pattern around these vessels reminiscent (though not as extensive) of the pattern in the sweet potato reference sample (Online Resource Figures 6.7c, 6.7d and 6.8a) can be seen in the virtual longitudinal sections (Fig. 5c, d). A single-factor ANOVA test found a significant difference between the archaeobotanical sample and the charred reference material in the periderm cell wall thickness, although the parenchyma cell wall thicknesses were not significantly different. This is to be expected given the extent of fused cells in the periderm and cortex. The full length of this fragment has been examined in transverse section for any signs of concentric rings of secondary growth. There are faint suggestions of the cellular structure around the xylem strands in places; however, the distortion and cavities created through charring create a high degree of uncertainty. More convincing is the overall anatomy of the fragment which is consistent with sweet potato. Recognisable periderm, cortex, vascular cylinder and parenchyma are all present (Fig. 5d–g) and a large portion of periderm/cortex bulges away from the surface (Fig. 5a–g).

Discussion

Key diagnostic features for identification

Hather (2000) recognised that various anatomical elements enable taxonomic determinations for fragments of archaeological parenchyma, ranging from gross morphological characteristics of culm fragments and USOs to microscopic cellular-scale features. Although taxonomic determinations are problematic for much archaeological parenchyma, often due to a lack of comparative reference material, they are more readily made when seeking to discriminate between particular genera and species. In this study, culm fragments required discrimination among groups of cane grass and bamboo, while USO fragments required discrimination between yams and sweet potato.

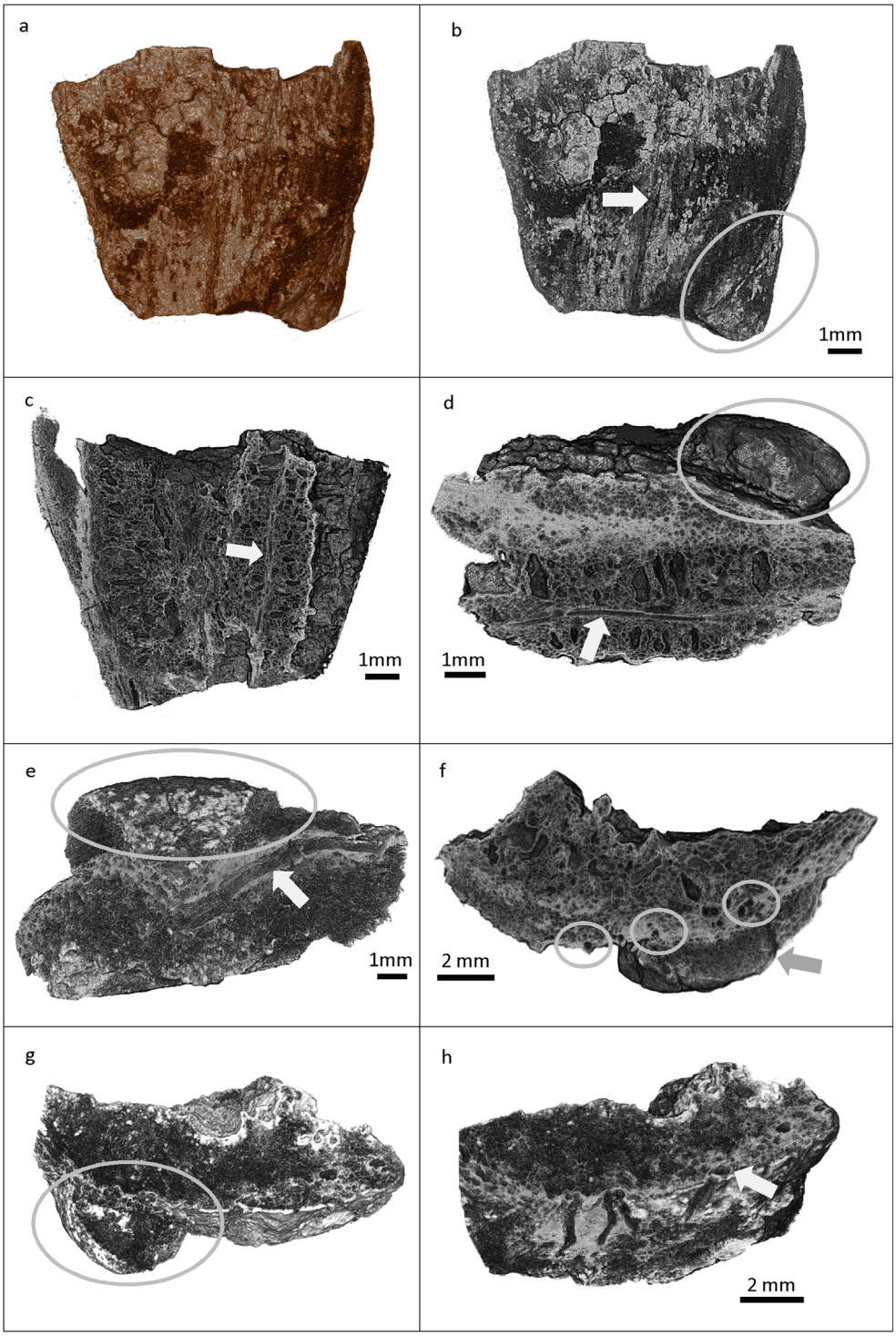

Fig. 5 MicroCT images of Fr16.3, F38. **a** Whole fragment in colour. **b** In greyscale—bulge of periderm/cortex (circled in **b**, **d**, **e** and **g**) and visible xylem strand in pith (indicated by arrow). **c** Internal plane—virtual tangential LS showing cavities created by charring around internal pith xylem vessel (indicated by arrow). **d** Internal plane—virtual radial LS showing cavities around xylem vessel within pith parenchyma created by charring **e** Internal plane—virtual radial LS showing xylem in cambial layer running the length of the fragment (indicated by arrow) below bulging periderm/cortex. **f** Internal plane—virtual TS showing periderm bulge (arrow) and VB (xylem vessels circled) in cambial layer. **g** Internal plane in transverse view—periderm bulging and peeling away from the surface (circled). **h** Internal plane—bulging periderm cropped away to expose vascular cambium in oblique transverse view. Arrow indicates one example of xylem in cambial layer

Cane grasses

As members of the same taxonomic family grouping, species of sugarcane and bamboo have morphological features in common. The key differentiating histological feature is the species-specific morphology of the vascular bundles surrounded by sclerenchyma bundle sheath fibre strands and their spatial arrangement, which can only be observed in transverse section.

The vascular bundles of sugarcanes may be described as uniformly rhomboid to ovate. While they vary in size and degree of surrounding sclerenchyma bundle sheath fibres across the culm, ranging from extensive at the culm periphery to minimal in the internode pith, a consistent configuration is

maintained. The metaxylem is larger relative to the protoxylem and never extends beyond the sclerenchyma bundle sheath margins (Metcalfe 1960). Images of reference specimens in Online Resource (Fig. 3) demonstrate this point for *Saccharum officinarum* and *Saccharum spontaneum* L. as representatives of the sugarcanes. The microCT virtual transverse sections of Fragments 20.2 and 20.6 (Online Resource Figs. 7.4, 7.6-7.8 and 7.11b) show anatomical features that are consistent with modern reference specimens.

In contrast, the configurations of vascular bundles and bundle sheaths in the bamboos have been classified into four types with subtypes that vary across and along the culm when viewed in transverse section (Grosser and Liese 1971; Liese 1998). An additional feature of the bamboos which does not occur in *S. officinarum* is the hollow at the centre of the internode culm (Mannan et al. 2017). Images of bamboo reference specimens in supplemental material (Online Resource Fig. 8) demonstrate these points for *Dendrocalamus giganteus* Wall. ex Munro, *Bambusa vulgaris* (Wahab et al. 2010), *Bambusa solomonensis* and *Neololeba atra* (Lindl.) Widjaja syn. *Bambusa forbesii* (Ridl.) Holttum.

Sweet potato and yams

The key diagnostic feature which separates the underground storage organs (USO) of dicotyledonous sweet potato *Ipomoea batatas* from the monocotyledonous yams of *Dioscorea* is the orientation and arrangement of the vascular tissue within the USO. *Dioscorea* tubers are characterised from the periphery inwards by one layer of cork cells, several rows of cortical cells, multiple meristematic cell layers and central ground parenchyma not unlike that of sweet potato (Ayensu 1972). However, the vascular tissue occurs randomly throughout the central core of parenchymatous tissue of the tuber. The general anatomy of a *D. nummularia* tuber is shown in supplemental material (Online Resource Fig. 5) representing *Dioscorea* yams. The surface of the whole tuber is rough with multiple stems of various diameters protruding from the surface (Online Resource Fig. 5.1). SEM images of cellular details (Online Resource Figs. 5.3–5.5) confirm the disorganised nature of parenchyma and vascular tissue inside the yam.

In contrast there is a very ordered structure throughout sweet potato with distinct layers of cells including the outer periderm, the cortex and the endodermis with a cambium layer containing vascular tissue arranged longitudinally in a cylinder which runs parallel to the outer surface (Hather and Kirch 1991). The general histological arrangement of the sweet potato is shown in Online Resource (Figs. 6). The orientation of the parenchyma in the cortex is tangential whereas it is radial inside the cambium (Hather and Kirch 1991) (Online Resource Figures 6.3a and 6.3b). In addition, sweet potato is noted for its secondary growth around the vascular tissue which creates a distinctive circular arrangement of concentric rings of parenchymatous cells (Esau 1977) around individual strands of xylem or phloem (McCormick 1916).

Assessment of microCT

MicroCT has proven a valuable tool for the investigation of archaeological parenchyma. It provides a high-resolution and non-destructive means through which archaeological parenchyma can be described for taxonomic determinations. Detailed virtual histology enables accurate descriptions of internal, as well as external, anatomical features. Thus, microCT is a major technological advance on the description of exterior surfaces of archaeobotanical samples using RLM and SEM. It also has advantages over histological slide and SEM stub preparations because it provides the same anatomical information without destruction of the sample.

In addition to its methodological advantages over standard techniques for the investigation of archaeological parenchyma, microCT has the capability to create online, virtual databases of entire archaeobotanical and reference samples. Thereby, reference databases can be shared without restriction globally for download and use, and datasets for entire archaeobotanical samples can be put online for comparative examination and reanalysis. The software platform to enable the virtual archaeological parenchyma database is currently under development.

Conclusion

Five fragments of archaeological parenchyma have been examined in detail by RLM and microCT scans. The identification of fragment 20.2 (feature 27) is confirmed as *Saccharum officinarum* with the highest level of confidence. It closely resembles published taxonomic descriptions, as well as RLM and SEM images of modern reference specimens both in diagnostic detail and metrics. Fragment 20.6 (feature 27) is most probably *Saccharum officinarum*. It also resembles published taxonomic descriptions and reference samples. This identification is less secure mainly because the fragment is incomplete and lacks the full spectrum of anatomical features that a culm periphery provides.

Fragment 61.9 (feature 32), fragment 16.3 (feature 38) and fragment 14.1 (feature 30) all show strong affinities with sweet potato (*Ipomoea batatas*). The nature of the charred cavities is consistent with published descriptions, as well as with RLM and SEM images of charred reference material created for this study. The ordered histological organisation closely resembles that of published descriptions and reference samples of sweet potato that confidently distinguish each of the three fragments from the reference sample of *Dioscorea nummularia*. However, it is not clear which prefix should be

applied to these identifications. While the morphological fit is highly consistent with reference charred sweet potato, histological metric analysis is unlikely to be reliable given the state of fusion of the cellular structure. Further study would be needed to rule out all species of *Dioscorea* given that most of their morphological and histological characteristics have yet to be described in detail.

We re-examined previously described and undescribed fragments to confirm previous identifications, as well as to provide a proof of concept for the application of microCT to the analysis of archaeological parenchyma. Comparable analyses would not have been possible with traditional RLM and SEM protocols, which do not enable internal 2D and 3D visualisations of the entire sample. Although some visualisations could be replicated using destructive histological section analysis, microCT is non-destructive. Following microCT analysis, the archaeobotanical samples are still intact and available for reanalysis in the future. In addition, the files created by the microCT scans are a permanent record which can be made available in a digital database to be re-examined at any time for educational purposes or by anyone wishing to verify the analysis and identifications.

Acknowledgments The authors thank for their assistance the following individuals: Professor Jack Golson for permission to undertake research on the archaeobotanical samples from Kuk Swamp; Dr. Rachel Wood (RSES, ANU) for assistance with AMS dating of two cane grass fragments; Professor Tim Senden, Director of the Department of Applied Mathematics (ANU) for supporting access to microCT facilities; Brendan Lepschi and Dave Albrecht from the Australian National Herbarium for the provision of herbarium reference material. We also acknowledge Rosemary White and Vivian Rolland, CSIRO Agriculture microscopy unit, for their expert advice. We thank Shane Paxton and John Vickers at the Research School of Earth Science, ANU, for reference sample preparation. Thanks also to Aleese Barron and Erica Seccombe for their instruction in Drishti image analysis.

Funding information The research was funded by an Australian Research Council (FT150100420) grant to TD.

Compliance with ethical standards

Conflicts of interest The authors declare that there are no conflicts of interest.

References

Antonio GC, Takeiti CY, Oliveira RA, de Park KJ (2011) Sweet potato: production, morphological and physicochemical characteristics, and technological process. Fruit Veg Cereal Sci Biotechnol 5:1–18

Ayensu ES (1972) Bulbil, tuber and rhizome. In: Metcalfe CR (ed) Anatomy of the monocotyledons VI. Discoreales. Clarendon Press, Oxford

Barron A, Turner AM, Beeching L, Bellwood P, Piper P, Grono E, Jones R, Oxenham M, Kien NKT, Senden T, Denham TP (2017) MicroCT reveals domesticated rice (*Oryza sativa*) within pottery sherds from early Neolithic sites (4150-3265 cal BP). Southeast Asia, Scientific Reports 7: 7410

Barton H, Paz V (2007) Subterranean diets in the tropical rain forests of Sarawak, Malaysia. In: Denham T, Iriarte J, Vrydaghs L (eds) Rethinking agriculture: archaeological and ethnoarchaeological perspectives. Routledge, Taylor and Francis Group, London, pp 50–77

Bello SM, De Groote I, Delbarre G (2013) Application of 3-dimensional microscopy and micro-CT scanning to the analysis of Magdalenian portable art on bone and antler. J Archaeol Sci 40:2464–2476

Booth TJ, Redfern RC, Gowland RL (2016) Immaculate conceptions: micro-CT analysis of diagenesis in Romano-British infant skeletons. J Archaeol Sci 74:124–134

Denham TP, Haberle SG, Lentfer C, Fullagar R, Field J, Therin M, Porch N, Winsborough B (2003) Origins of agriculture at Kuk Swamp in the Highlands of New Guinea. Science 301:189–193

Denham TP, Atchison J, Austin J, Bestel S, Bowdery D, Crowther A, Dolby N, Fairbairn A, Field J, Kennedy A, Lentfer C, Matheson C, Nugent S, Parr J, Prebble M, Robertson G, Specht J, Torrence R, Barton H, Fullagar R, Haberle S, Horrocks M, Lewis T, Matthews P (2009) Archaeobotany in Australia and New Guinea: practice, potential and prospects. Aust Archaeol 68:1–10

Edwards T, Grono E, Herries AIR, Brink FJ, Troitzsch U, Senden T, Turner M, Barron A, Prossor L, Denham TP (2017) Visualising scales of process: multi-scalar geoarchaeological investigations of microstratigraphy and diagenesis at hominin bearing sites in South African karst. J Archaeol Sci 83:1–11

Esau K (1977) The anatomy of seed plants, 2nd edn. Wiley, New York

Golson J, Denham TP, Hughes PJ, Swadling P, Muke J (eds) (2017) Ten thousand years of cultivation at Kuk Swamp in the highlands of Papua New Guinea. Terra Australis 46. ANU E Press, Canberra

Grosser D, Liese W (1971) On the anatomy of Asian bamboos, with special reference to their vascular bundles. Wood Sci Technol 5: 290–312

Haneca K, Deforce K, Boone MN, Van Loo D, Dierick M, Van Acker J, Van Den Bulcke J (2012) X-ray sub-micron tomography as a tool for the study of archaeological wood preserved through the corrosion of metal objects. Archaeometry 54:893–905

Hather JG (1988) The morphological and anatomical interpretation and identification of charred vegetative parenchymatous plant remains. Unpublished PhD thesis, University College London

Hather JG (1991) The identification of charred archaeological remains of vegetative parenchymatous tissue. J Archaeol Sci 18:661–675

Hather JG (1992) The archaeobotany of subsistence in the Pacific. World Archaeol 24:70–81

Hather JG (1994a) A morphological classification of roots and tubers and its bearing on the origins of agriculture in Southwest Asia and Europe. J Archaeol Sci 21:719–724

Hather JG (1994b) The identification of charred root and tuber crops from archaeological sites in the Pacific. In: Hather JG (ed) Tropical archaeobotany: applications and new developments. Routledge, London, pp 51–64

Hather JG (1996) The origins of tropical vegeculture: Zingiberaceae, Araceae and Dioscoreaceae in Southeast Asia. In: Harris DR (ed) The origins and spread of agriculture and pastoralism in Eurasia. University College London Press, London, pp 538–550

Hather JG (2000) Archaeological parenchyma. Archaeotype Publications, London

Hather JG, Kirch PV (1991) Prehistorical sweet potato (*Ipomoea batatas*) from Mangaia Island, Central Polynesia. Antiquity 65:887–893

Horrocks M, Grant-Mackie J, Matisoo-Smith E (2008) Introduced taro (*Colocasia esculenta*) and yams (*Dioscorea* spp.) in Podtanean (2700–1800 years BP) deposits from Mé Auré Cave (WMD007), Moindou, New Caledonia. J Archaeol Sci 35:169–180

Ladefoged TN, Graves MW, Coil JH (2005) The introduction of sweet potato in Polynesia: early remains in Hawai'i. J Polynesian Soc 114: 359–373

Lewis T, Denham TP, Golson J (2016) A renewed archaeological and archaeobotanical assessment of house sites at Kuk Swamp in the highlands of Papua New Guinea. Archaeol Ocean 51:91–103

Liese W, (1998) The anatomy of bamboo culms. International Network for Bamboo and Rattan, Beijing, Eindhoven, New Delhi

Limaye A, (2012) Drishti: a volume exploration and presentation tool. Proceedings of the International Society for Optics and Photonics. Developments in X-Ray Tomography VIII, 8506

Mannan S, Paul Knox J, Basu S, (2017) Correlations between axial stiffness and microstructure of a species of bamboo. R Soc Open Sci 4

McCormick FA (1916) Notes on the anatomy of the young tuber of *Ipomoea batatas* Lam. Bot Gaz 61:388–398

Metcalfe CR (1960) Anatomy of the monocotlyledons. I. Gramineae. Oxford University Press, Oxford

Oliveira N, (2008) Subsistence archaeobotany: food production and the agricultural transition in East Timor. Unpublished PhD thesis, Australian National University

Paz V, (2001) Archaeobotany and cultural transformation: patterns of early plant utilisation in northern Wallacea. Unpublished PhD thesis, University of Cambridge

Philpott M, Ferguson LR, Gould KS, Harris PJ (2009) Anthocyanidin-containing compounds occur in the periderm cell walls of the storage roots of sweet potato (*Ipomoea batatas*). J Plant Physiol 166: 1112–1117

Reimer PJ, Bard E, Bayliss A, Beck J, Blackwell PG, Bronk Ramsey C, Buck CE, Cheng H, Edwards RL, Friedrich M, Grootes PM, Guilderson TP, Haflidason H, Hajdas I, Hatte C, Heaton TJ, Hoffmann DL, Hogg AG, Hughen KA, Kaiser KF, Kromer B, Manning SW, Niu M, Reimer RW, Richards DA, Scott EM, Southon JR, Staff RA, Turney CSM, van der Plicht J (2013) IntCal13 and MARINE13 radiocarbon age calibration curves 0-50, 000 years calBP. Radiocarbon 55(4):1869–1887

Rosendahl P, Yen D (1971) Fossil sweet potato remains from Hawaii. J Polynesian Soc 80:379–385

Stelzner J, Million S (2015) X-ray computed tomography for the anatomical and dendrochronological analysis of archaeological wood. J Archaeol Sci 55:188–196

Stuiver M, Reimer PJ, Reimer RW, (2005) CALIB 5.0 [program and documentation]

Talbot MJ, White RG (2013) Methanol fixation of plant tissue for scanning electron microscopy improves preservation of tissue morphology and dimensions. Plant Methods 9:36. https://doi.org/10.1186/1746-4811-9-36

Ugent D, Peterson LW (1988) Archaeological remains of potato and sweet potato in Peru. Int Potato Cent Circ 16:1–10

Ugent D, Pozorski S, Pozorski T (1981) Prehistoric remains of the sweet potato from the Casma Valley of Peru. Phytologia 49:401–415

Ussher E, (2015) Agricultural development in Tongan prehistory: an archaeobotanical perspective, PhD thesis, Australian National University, p. 335

Varslot T, Kingston A, Myers G, Sheppard A (2011) High-resolution helical conebeam micro-CT with theoretically-exact reconstruction from experimental data. Med Phys 38:5459–5476

Wahab R, Mohd Tamizi M, Sulaman O, Mohamed A, Hassan A, Khalid I (2010) Anatomical and physical properties of cultivated two and four year old *Bambusa vulgaris*. Sains Malaysiana 39:571–579

Whitau R, Dilkes-Hall IE, Dotte-Sarout E, Langley MC, Balme S, O'Connor S (2016) X-ray computed microtomography and the identification of wood taxa selected for archaeological artefact manufacture: rare examples from Australian contexts. J Archaeol Sci Rep 6: 536–546